

Chemical telemetry of OH observed to measure interstellar magnetic fields

Serena Viti¹ Thomas W. Hartquist² and Philip C. Myers³

Department of Physics and Astronomy, University College London, London WC1E 6BT,
UK sv@star.ucl.ac.uk

School of Physics and Astronomy, University of Leeds, Leeds LS2 9JT, UK

Harvard - Smithsonian Center for Astrophysics, 60 Garden Street, Cambridge MA 02138,
USA

Abstract

We present models for the chemistry in gas moving towards the ionization front of an HII region. When it is far from the ionization front, the gas is highly depleted of elements more massive than helium. However, as it approaches the ionization front, ices are destroyed and species formed on the grain surfaces are injected into the gas phase. Photodissociation removes gas phase molecular species as the gas flows towards the ionization front. We identify models for which the OH column densities are comparable to those measured in observations undertaken to study the magnetic fields in star forming regions and give results for the column densities of other species that should be abundant if the observed OH arises through a combination of the liberation of H₂O from surfaces and photodissociation. They include CH₃OH, H₂CO, and H₂S. Observations of these other species may help establish the nature of the OH spatial distribution in the clouds, which is important for the interpretation of the magnetic field results.

keywords ISM: HII regions, magnetic fields, molecules - masers - stars: formation

1 Introduction

It is not yet clear whether clouds are generally magnetically supercritical or subcritical in the sense that the mass-to-magnetic flux ratio is above or below the critical value at which gravity overcomes the support by the magnetic field (Mouschovias & Spitzer 1976). What is clear, however, is that this distinction is very important, as the mode of star formation depends on whether a cloud is magnetically supercritical or subcritical (e. g. Shu et al. 1987). Measurements of interstellar magnetic field strengths in molecular clouds are vital.

Crutcher (1999) produced a detailed compilation of reliable results, obtained up to the time of his writing, for line - of - sight magnetic field strengths and upper limits inferred from observations of OH in a sample of molecular clouds. He also collected data on column densities, line widths, number densities, temperatures, and molecular cloud sizes. Crutcher (1999) concluded that the values of the mass - to - magnetic flux ratios are about twice the critical value. Shu et al. (1999) compared the data with a model of a highly flattened cloud (Allen & Shu 2000) and inferred that the mass -

to - flux ratios have values that are approximately equal to the critical value. Bourke et al. (2001) have obtained further OH and column density data and performed a related analysis and they concluded that their results are model dependent: if the model cloud is initially a uniform sphere with a uniform field strength then the cloud is magnetically supercritical. If instead, the model cloud is a flattened sheet, the data imply that the system is stable. In general, their detection rate was low and they explained this as a result of a selection effect: most of their sources were towards H II regions that are probably expanding; the expansion of an H II region leads to the compression of the surrounding gas into a thin shell-like structure, decreasing the Zeeman effect. This tends to make clouds that are not necessarily magnetically supercritical appear as though they are.

The analysis to determine the dynamical significance of the measured line - of - sight magnetic field strengths are based on the assumption that the OH Zeeman data provide a measure of the magnetic field strength throughout the region where most of the material, contributing to the column density, is. However, the possibility that OH is particularly abundant in restricted shells around HII regions has been suggested (Elitzur & de Jong 1978; Hartquist et al. 1995) in work on maser sources. Due to the spatial coincidence of OH and CH₃OH maser sources in W3(OH) established by Menten et al. (1992), Hartquist et al. (1995) argued that the release of icy mantles from grain surfaces in gas moving towards an ionization front plays a major role in the chemistry in the maser regions. CH₃OH is a direct product of the surface chemistry, and OH is generated through the photodissociation of H₂O injected into the gas phase from the surfaces. Crutcher (2004, private communication) has argued that the absence of limb brightening and other observational results demonstrate that in some sources, for which the OH data yield clear measurements of the magnetic field strength, the OH is not primarily concentrated in shells. However, he does accept the possibility that in at least some of the sources for which the studies yield only upper limits for the field strengths, OH may be mostly in shells. This might contribute to the null detections of the Zeeman effect in some sources.

The main motivation of this paper is an attempt to develop a means to establish whether in some cases OH, used in measurements of magnetic field strengths, exists in rather localized regions as a consequence of forming in photodissociation regions. Our study shows that it is indeed possible to produce OH with a column density in the range of those measured by Bourke et al. (2001) in the manner described by Hartquist et al. (1995). We have developed the model in the first step in an attempt to chemically determine whether the molecular gas around H II regions may indeed be swept up into thin shells, resulting in a nonuniform magnetic field geometry, that leads to measured values of the field strength that are much lower than the true values. If the OH is formed as gas approaches the ionization front, our model allows the prediction of the column densities of other species that may be observed to confirm the validity of the model. Measured column densities for these other species that disagree with the predictions would suggest that the OH is not primarily in gas near the ionization front.

In section 2 we describe the model assumptions. Section 3 contains our results and discussion, and Section 4 concludes the paper.

2 Description of the Model

The basic chemical model we adopt is a modification of the model employed in Viti et al. (2003). The chemical network is taken from the UMIST database (Millar et al. 1997; Le Teuff et al. 2000). We follow the chemical evolution of 168 species involved in 1777 gas-phase and grain reactions. This paper presents the first results of such an extensive chemical model for shells in which OH is particularly abundant. Other potentially observable species were not considered by Elitzur & de Jong (1978), and Hartquist et al. (1995) did not give quantitative results, even for CH₃OH, relevant to the picture investigated here. The model calculation is carried out in two phases, both of which are time-dependent. In Phase I, the clump of gas is formed during the gravitationally driven collapse of an initially diffuse molecular region from a hydrogen nucleus number density, n_H , to a much higher fixed final number density. Free-fall collapse is assumed. During this phase, gas-phase chemistry and freeze out on to dust grains with subsequent processing (mainly hydrogenation) are assumed to occur (see Viti et al. 2003 for a full description). The initial density of the clump is taken to be 500 cm⁻³ while the final density, n_f , is treated as a free parameter. Note that the initial density is consistent with observations of the Rosette molecular cloud translucent clumps (Williams, Blitz & Stark 1995). We have run a test model where the initial density was set to 100 cm⁻³: the final abundances of the collapsed clump do not seem to be significantly affected. Hence, we have taken 500 cm⁻³ as our initial density for all models.

The gas then remains motionless for some time and subsequently, in Phase II, begins to move at a constant velocity, v , towards an ionization front. The time for which the gas remains motionless is determined by the extent to which we wish depletion to occur for the particular run. At the time at which motion towards the front begins, the visual extinction, A_V , of material between the location of the parcel of gas under consideration and the ionization front is 10 mags.

The relationship between the visual extinction and the distance to the ionization front, $z(t)$, at time t is taken to be

$$A_V = n_H \times z(t) / 1.6 \times 10^{21} \text{ cm}^{-2} \quad (1)$$

The radiation field at the ionization front is assumed to be χ times the standard unshielded mean interstellar radiation background of Habing (1968).

At the time Phase I is over, a percentage, FR, of the nuclei of elements more massive than helium initially in the gas phase has frozen - out. In Table 2 we show the surface abundances of several species at the beginning of Phase II for one of the models. During this latter phase, as the gas moves towards the ionization front, A_V decreases until the gas is unshielded enough (at $A_{V, \text{evap}}$) that all surface material is returned instantaneously to the gas phase. The assumption of instantaneous evaporation is motivated in this context by the high radiation fields involved: the Viti et al. (2003) models imply that the enhanced molecular condensations ahead of Herbig-Haro objects, where the radiation field is higher than ambient but certainly lower than the radiation fields considered here, can only come from evaporated icy mantles which are rapidly injected into the gas phase.

Thus the free parameters are n_f , FR, χ , $A_{V, \text{evap}}$, and v . A further free parameter is the fraction of CO converted into methanol on the surface of the grains. How-

ever, on the basis of CH₃OH absorption observations (Menten et al. 1986) and OH maser models (e. g. Gray et al. 1992) we know that CH₃OH has an abundance comparable to or even greater than that of OH. There is no known gas phase mechanism at low temperatures that produces quantities of CH₃OH comparable to those found in CH₃OH maser sources. Surface chemistry is almost certainly involved in the production of CH₃OH.

By running a model (Model 0, see Table 1) which simulates the maser environment ($n_H = 10^7 \text{ cm}^{-3}$, $T = 50 \text{ K}$; $\chi = 3 \times 10^5$) we found that the CH₃OH column density is comparable to the OH column density only if at least 25% of the carbon monoxide sticking on the grains is converted into methanol. Hence, for all the models presented here we have assumed that 25% of CO is converted into CH₃OH on grains.

The dynamical description that we have used is equally applicable to a situation in which, in the frame of reference of the star, the ionization front is expanding at speed v towards a gas that is motionless, or to a situation in which the gravity of the star causes gas to fall at a speed of v towards the star and approach an ionization front that is not moving in the star's frame (cf. Keto 2002). In the Keto (2002) dynamical model of HII region, infall through a static front would maintain the overall dynamical and chemical structures near the front for close to the entire lifetime of an HII region.

We have explored a large parameter space resulting in 33 models. However, after a preliminary analysis, and for simplicity, we decided to list here only the most plausible ones (see Table 1). Note that we have retained only those models where Phase II begins with highly depleted material, which we believe is quite realistic because some dense cores, in regions where high mass stars have not started to form, have CO fractional abundances that are close to two orders of magnitude below those elsewhere (e.g. Caselli et al. 2002). Those cores almost certainly form on a timescale comparable to that of the free-fall time and may well remain quiescent for some time. The regions that we are modelling here have densities that are within a factor of a few to ten of those of the dense cores mentioned above and may well have dynamical and chemical histories similar to those of the dense cores as well.

3 Results and Discussion

Bourke et al. (2001) derived column densities for OH in the range of 4×10^{14} to $3 \times 10^{15} \text{ cm}^{-2}$. For many models for which FR is 25% or 50% (not shown), the OH column density between $A_V = 10$ and $A_V = A_{V, \text{evap}}$ is greater than the OH column density for A_V less than $A_{V, \text{evap}}$. We wish to examine the possibility that the absorption occurs primarily near the ionization front. Thus, we consider here only models for which FR = 100%.

Table 1 gives values of the parameters specifying each model. Table 2 gives the column density of various species between $A_V = 10$ mags (the beginning of Phase II) and A_V equal to the value given in the final column; in Figure 1 the fractional abundances of OH for selected models are shown as a function of A_V , always after the grain mantles have evaporated, up to $A_V \sim 3.5$ mags, corresponding to a post-evaporation timescale of the order of 3×10^4 – 3×10^5 years.

From Figure 1, we see that soon after evaporation, OH is very abundant for all models: this is due to the evaporation of water which efficiently dissociates. OH is

Table 1: Model Parameters. The notation a(b) signifies $a \times 10^b$. The model number is listed in Column 1; Column 2 shows the density of the gas at the end of Phase I; Columns 3, 4 and 5 list respectively the velocity of the clump, the strength of the radiation field and the visual extinction at which the grains evaporate during Phase II. For all models listed here FR = 100% and 25% of CO is converted into CH₃OH on the grains.

Model	n_f (cm ⁻³)	v (km/s)	χ	$A_{V_{evap}}$
0	1(7)	1	3(5)	8
1	1(5)	1	3(3)	8
2	1(5)	2	3(3)	8
3	1(5)	1	3(4)	8
4	1(5)	2	3(4)	8
5	1(5)	1	3(3)	6
6	1(5)	1	3(4)	6
7	1(4)	1	3(3)	6
8	1(4)	1	3(3)	5
9	1(5)	1	3(4)	5

Table 2: Surface fractional abundances of several species at the beginning of Phase II for Model 8.

H ₂ O	4(-4)
CO	1(-5)
H ₂ CO	6(-8)
CH ₃ OH	4(-6)
H ₂ S	1(-5)
NH ₃	3(-5)
CH ₄	2(-4)
N ₂	1(-5)

Table 3: Column densities of selected species for Models 1-9, calculated from 10 mags to the A_V shown in column 11.

Model	OH	CO	HCO ⁺	H ₂ CO	H ₂ S	SO	SO ₂	CH ₃ OH	NH ₃	A_V
1	1.451(17)	4.781(17)	3.212(12)	4.113(15)	2.066(16)	2.933(15)	1.807(16)	2.773(15)	5.518(16)	2
1	1.451(17)	4.483(17)	3.210(12)	4.113(15)	2.066(16)	2.933(15)	1.807(16)	2.773(15)	5.518(16)	4
1	1.448(17)	5.448(16)	3.338(11)	2.903(15)	2.064(16)	1.921(15)	1.697(16)	2.765(15)	5.515(16)	6
1	—	—	—	—	—	—	—	—	—	8
2	1.835(17)	4.379(17)	3.647(12)	4.699(15)	2.705(16)	3.089(15)	1.858(16)	3.584(15)	7.300(16)	2
2	1.835(17)	3.745(17)	3.645(12)	4.699(15)	2.705(16)	3.089(15)	1.858(16)	3.584(15)	7.300(16)	4
2	1.731(17)	3.253(16)	4.375(10)	2.431(15)	2.670(16)	7.600(14)	1.242(16)	3.493(15)	7.216(16)	6
2	—	—	—	—	—	—	—	—	—	8
3	6.900(16)	4.354(17)	2.983(12)	1.949(15)	5.967(15)	2.426(15)	9.724(15)	7.965(14)	1.512(16)	2
3	6.900(16)	4.349(17)	2.983(12)	1.949(15)	5.967(15)	2.426(15)	9.724(15)	7.965(14)	1.512(16)	4
3	6.899(16)	2.121(17)	2.964(12)	1.940(15)	5.967(15)	2.426(15)	9.724(15)	7.965(14)	1.512(16)	6
3	—	—	—	—	—	—	—	—	—	8
4	1.094(17)	4.008(17)	3.603(12)	2.525(15)	9.391(15)	2.847(15)	1.208(16)	1.245(15)	2.420(16)	2
4	1.094(17)	4.002(17)	3.602(12)	2.525(15)	9.391(15)	2.847(15)	1.208(16)	1.245(15)	2.420(16)	4
4	1.094(17)	1.419(17)	3.292(12)	2.415(15)	9.391(15)	2.846(15)	1.208(16)	1.245(15)	2.420(16)	6
4	—	—	—	—	—	—	—	—	—	8
5	3.377(16)	3.625(17)	2.066(12)	1.720(15)	1.766(15)	1.300(15)	4.637(15)	2.837(14)	4.934(15)	2
5	3.377(16)	3.340(17)	2.065(12)	1.720(15)	1.766(15)	1.299(15)	4.637(15)	2.837(14)	4.934(15)	4
5	—	—	—	—	—	—	—	—	—	6
5	—	—	—	—	—	—	—	—	—	8
6	3.501(15)	1.764(17)	6.503(11)	2.673(14)	3.346(14)	2.172(14)	3.233(14)	4.463(13)	9.157(14)	2
6	3.501(15)	1.759(17)	6.497(11)	2.673(14)	3.346(14)	2.172(14)	3.233(14)	4.463(13)	9.157(14)	4
6	—	—	—	—	—	—	—	—	—	6
6	—	—	—	—	—	—	—	—	—	8
7	5.857(15)	1.838(17)	9.236(11)	3.081(14)	2.155(14)	2.731(14)	3.512(14)	8.331(13)	4.723(14)	2
7	5.857(15)	1.833(17)	9.230(11)	3.081(14)	2.155(14)	2.731(14)	3.512(14)	8.331(13)	4.723(14)	4
7	1.253(12)	—	—	—	—	—	—	—	—	6
7	1.037(12)	—	—	—	—	—	—	—	—	8
8	1.533(14)	4.130(16)	7.094(10)	2.839(13)	1.582(14)	6.318(12)	2.127(12)	4.739(13)	3.316(14)	2
8	1.532(14)	4.086(16)	7.035(10)	2.838(13)	1.582(14)	6.303(12)	2.127(12)	4.739(13)	3.316(14)	4
8	1.253(12)	—	—	—	—	—	—	—	—	6
8	1.037(12)	—	—	—	—	—	—	—	—	8
9	9.037(11)	3.717(16)	9.703(09)	9.748(12)	3.433(14)	7.221(11)	1.018(12)	4.147(13)	9.391(14)	2
9	8.849(11)	3.672(16)	9.118(09)	9.737(12)	3.433(14)	7.066(11)	1.018(12)	4.147(13)	9.391(14)	4
9	—	—	—	—	—	—	—	—	—	6
9	—	—	—	—	—	—	—	—	—	8

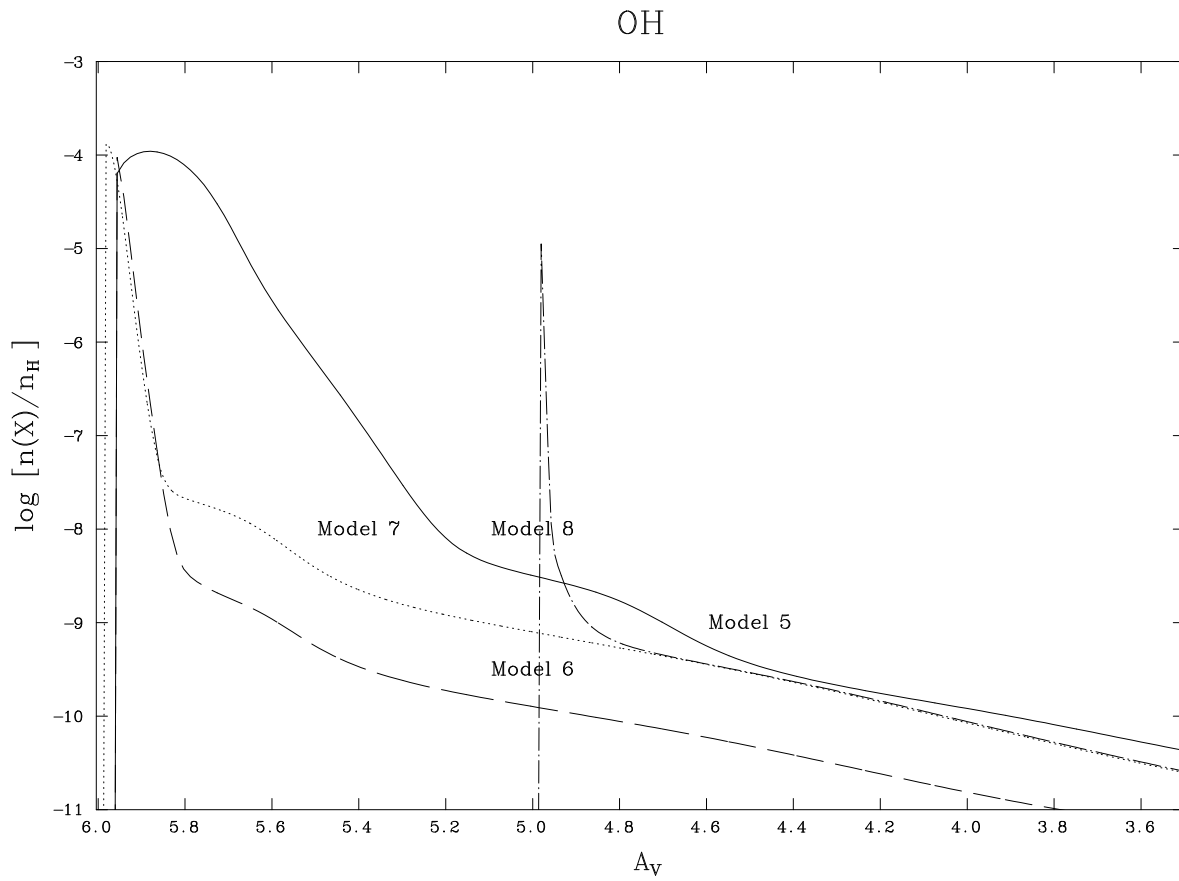


Figure 1: Fractional abundance of OH for selected models as a function of A_V .

then destroyed, also by photodissociation. We note that a high radiation field (e.g. Model 6) or a low $A_{V,evap}$ (e.g. Model 8) accelerates the destruction of OH. Moreover, another consequence of a high χ is also a very fast destruction of most gas phase species.

From Table 2, we note that Models 6, 7 and 8, are the only ones for which the OH column densities from $A_V = 0$ to 10 mags are comparable to those measured by Bourke et al. (2001). For all three of these models $v = 1 \text{ km s}^{-1}$. The values of χ are 3×10^4 and 3×10^3 , which are within the range expected for early B and late O type stars at the distances that the ionization fronts of HII regions are from the central stars. The sensitivity of the results to the adoption of different values of $A_{V,evap}$ is demonstrated by a comparison of the results for Models 7 and 8. $A_{V,evap}$ has values of 6 and 5, respectively, for those models. A value of $A_{V,evap}$ similar to these is compatible with the inferences drawn by Viti et al. (2003) in their modelling of chemistry triggered by UV radiation emitted in shocks associated with Herbig - Haro objects.

Little contribution to the OH column density comes from the region where A_V is less than 4 mags. Inspection of Figure 1 of Hartquist & Sternberg (1991) shows that the OH in the present models is, thus, in regions where the temperature does not greatly exceed 10 K: this inference can be drawn solely from the high density results from Hartquist & Sternberg (1991) because for a fixed value of χ/n , the temperature, as a function of A_V , does not vary significantly at $A_V > 2$ mags. For fixed $A_V < 1$ mag and for fixed χ/n , the temperature increases with density due mostly to the collisional de-excitation of radiatively pumped H_2 becoming more important with increasing density. Nevertheless, in order to confirm this inference, we ran two test models with the UCL PDR code (Bell et al. 2005; Papadopoulos et al. 2002) at densities of 10^4 and 10^6 cm^{-3} . The results of these tests are shown in Figure 2. From this figure, it is clear that, while the temperature is high at the outer edge, at $A_V > 4$ mags, the temperature has values well below 100K and close enough to 10 K for this assumption to be appropriate for the chemical calculations. Note that the UCL PDR code and the chemical code used for the calculation of the grids reported in this paper are two versions of the same basic code. The main difference is, of course, in the treatment of the temperature: it is given as an input in the chemical code, while it is self-consistently computed in the UCL PDR code. The latter code has been recently benchmarked against many other PDR codes (Roellig et al. in prep).

Clearly the highest fractional abundances of OH and of other species is obtained only in a narrow A_V range near $A_{V,evap}$. This result justifies our adoption of plane parallel geometry.

If the observed OH towards the Bourke et al. sources is indeed caused by grain evaporation in parcels of gas moving toward the ionization front, then it would be desirable to find other tracers of this process. In particular, we note that CH_3OH should also be enhanced as a direct consequence of grain evaporation. From Table 2, it is clear that CH_3OH is always less abundant than OH for models 6 to 8, though in Model 0, which gives a column density of OH in the range of those in OH masers, the CH_3OH and OH column densities are similar. For models 6 to 8, the highest column density of CH_3OH is reached for Model 7, while for these three models the densities of OH and CH_3OH differ by the smallest factor in Model 8.

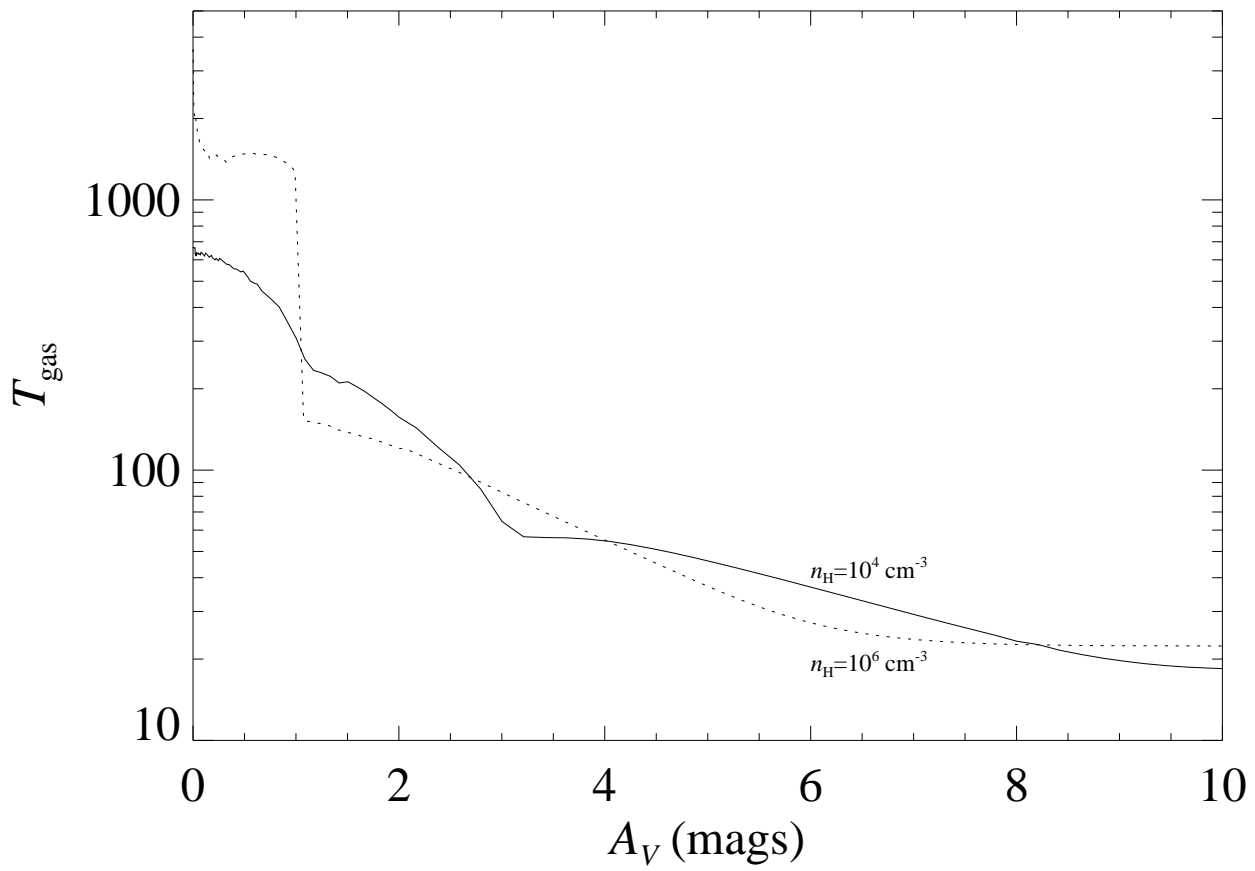


Figure 2: Gas temperature as a function of visual extinction for $n_H = 10^4 \text{ cm}^{-3}$, $\chi = 10^3$ Habing (solid line) and $n_H = 10^6 \text{ cm}^{-3}$, $\chi = 10^3$ Habing (dotted line)

4 Conclusions

In this paper we have put forward and explored the possibility that the OH absorption observed toward HII regions is due to the evaporation of grain mantles primarily near the HII regions' ionization fronts.

We show that it is possible for most of the detected OH to be in such locations provided that the grain mantles evaporate *before* the gas becomes completely unshielded to the strong radiation fields typical of these environments. In order to test this idea, additional absorption observations are desirable for the lines-of-sight for which Zeeman measurements of magnetic fields are made. They should be made in the lines of species that are often not abundant in cold dark cloud material but are abundant in the models presented here that give OH column densities near those measured by Bourke et al. (2001). In this respect CH₃OH and H₂S are particularly promising species, although a high column density of methanol is only obtained if a substantial amount of CO is converted into CH₃OH on the grains before evaporation. Methanol is routinely observed towards regions of high mass star formation, particularly towards UCHII regions, where it is mainly detected in maser emission (e. g. Walsh et al. 1997), and hot cores. H₂CO is also regularly observed in absorption, and the model results suggest that it too would be a good candidate for observations in appropriate directions. In fact, Downes et al. (1980) reported low spatial resolution observations of H₂CO towards several galactic sources and found that, at least in some cases, it is seen at the same velocity as the OH absorption. The high abundance of CH₃OH, H₂S and H₂CO are all a consequence of hydrogenation of simpler species on the grains during the collapse phase; once $A_{V, \text{evap}}$ is reached, hydrogenated species in the gas phase are enhanced. In the case of methanol, there is an additional contribution from the high radiation field which causes a high abundance of CH₃⁺; the latter efficiently reacts with water (also enhanced on the grains during the collapse phase) and forms the ion CH₃OH₂⁺ which then produces methanol via electronic recombination.

5 Acknowledgements

SV acknowledges individual financial support from a PPARC Advanced Fellowship. The collaboration was supported by a PPARC Visitors Grant held in Leeds.

6 References

- Allen, A., Shu, F. H. 2000, ApJ, 536, 368
Bell, T, Viti, S, Williams, D A, Crawford, I A, Price R J, 2005, 357, 961
Bourke, T. L., Myers, P. C., Robinson, G., Hyland, R. 2001, ApJ, 554, 916
Caselli, P., Walmsley, C. M., Zucconi, A., Tafalla, M., Dore, L., Myers, P. C., 2002, ApJ, 565, 344
Crutcher, R. M. 1999, ApJ, 520, 706
Downes, A. J. B., Wilson, T. L., Bieging J., Wink, J., 1980, A&AS, 40, 379
Elitzur, M., de Jong, T. 1978, A&A, 67, 323
Gray, M. D, Field, D., Doel, R. C. 1992, A&A, 262, 555
Habing, H. J. 1968, BAN, 20, 177

Hartquist, T. W., Sternberg, A. 1991, MNRAS, 248, 48
Hartquist, T. W., Menten, K. M., Lepp, S., Dalgarno, A. 1995, MNRAS, 272, 184
Keto, E. 2002, ApJ, 580, 980
Le Teuff, Y. H., Millar, T. J., Markwick, A. J. 2000, A&AS, 146, 157
Menten, K. M., Walmsley, C. M., Henkel, C, Wilson, T. L. 1986, A &A, 157, 318
Menten, K. M., Reid, M. J., Pratap, P., Moran, J. M., Wilson, T. L. 1992, ApJ, 401, L39
Millar, T. J., Farquhar, P. R. A., Willacy, K. 1997, A&AS, 121, 139
Mouschovias, T. Ch., Spitzer, L. Jr. 1976, ApJ, 210, 236
Papadopoulos, P, P, Thi, W.-F.; Viti, S, 2002, ApJ, 579, 270
Shu, F. H., Adams, F. C., Lizano, S. 1987, ARA&A, 25, 23
Shu, F. H., Allen, A., Shang, H., Ostriker, E. C., Li, Z.-Y. 1999, in The Origin of Stars and Planetary Systems, ed. C. J. Lada & N. D. Kylafis (Dordrecht: Kluwer), 193
Stantcheva, T., Caselli, P., Herbst, E. 2001, A&A, 375, 673
Viti, S., Girart, J. M., Garrod, R., Williams, D. A., Estalella, R. 2003, A&A, 399, 187
Walsh, A. J., Hyland A. R., Robinson G., Burton M. G., 1997, MNRAS, 291, 261
Williams, J. P., Blitz, L., Stark, A. A., 1995, ApJ, 451, 252